Joint Special Interest Group meeting between euspen and ASPE
Advancing Precision in Additive Manufacturing
TU Berlin, Germany, October 2025
www.euspen.eu

Validation of Melt Pool Prediction in Laser Powder Bed Fusion Using OpenFOAM

Mahmoud Al-Rashidi[1]*, Baoshun Zhou[2], Robert Kay[1], Mohamad Bayat[2], Masoud Jabbari[1]

[1]School of Mechanical Engineering, University of Leeds, Leeds, UK
[2]Department of Civil and Mechanical Engineering, Technical University of Denmark, Lyngby, Denmark

*kwtz9222@leeds.ac.uk

Abstract
A simulation of a single-track laser on 316L stainless steel was conducted using OpenFOAM (LaserbeamFoam) that is designed to simulate the Laser Powder Bed Fusion (PBF-L) process. The main objective is to predict the melt pool dimensions, specifically the width and depth, under typical L-PBF conditions. The results were compared against publicly available experimental data for validation. The simulation was performed on a 3D substrate with a moving Gaussian heat source applied to simulate the laser beam. Material properties such as density, specific heat, temperature dependent thermal conductivity are incorporated in the model. In addition, absorptivity parameters specific to the laserbeamFoam solver were included to improve the reliably of melt pool predictions. Key process parameters such as laser power, beam radius and scanning speed were selected to match those reported in the referenced study. The simulation results showed that the developed model can capture the primary thermal behaviour that governs the melt pool formation, with a relatively good level of agreement when compared with the experimental data. This solver has the capability to predict the melt pool morphology of L-PBF which is essential to optimise process parameters, to prevent process induced flaws like lack of fusion or keyholing. the simulated results shows that the width and depth of the melt pool get smaller as the scanning speed increases and the laser power increases. Depth predicted is within the range of experimental error, however the width is overestimated. Future work may consider modelling absorptivity as a function of temperature and phase changes, but such changes would demand considerable computational cost.

Simulation , OpenFOAM, LaserbeamFoam, PBF-L, Metal Additive Manufacturing, Melt Pool Morphology

1. Introduction

Sectors such as aerospace, biomedical, energy and automotive are sectors that have high standards and demands continuous improvement in their manufactured parts so manufacturing industry need to adopt to those standards and improve their precision, efficiency and capabilities. Creating complex metal components with minimum post processing is a major challenge in these sectors, driving continuous improvement in laser powder bed Fusion (L-PBF) technologies for metals such as 316L stainless steel. Reliable prediction of melt pool geometry during a single-track exposure is a key method for determining process control parameters, as melt pool width and depth significantly influence on the resultant part's mechanical properties, residual stresses and defect formation in the printed part [1,2]. Deviations from the desired geometry can result in part rejection since they do not meet required industrial standard.

This paper addresses the following: how accurate can LaserbeamFoam [3,4], an OpenFOAM based application predict the melt pool dimensions of a single laser track on 316L stainless steel compared to a published experimental paper. The focus here on melt pool morphology predicts width and depth.

Previous studies have used different numerical approaches such as semi-analytical models to generate fully-coupled thermal-fluid simulations that can estimate the melt pool behaviour [5–8]. while semi-analytical models have the benefit of computational speed, they are sacrificing the fidelity in capturing the transient thermal gradient. L-PBF simulation fidelity requires capturing the multiphasic aspects associated with the process specifically the coupling of fluid flow with effects like recoil pressure and Marangoni effect which laserbeamFoam consider[3]. LaserbeamFoam utilizes ray tracing technologies to discretise the laser heat source (Gaussian) to multiple rays using Fresnel equations to calculate the absorptivity expected at that incident angle [3]. Moreover, it incorporates some temperature dependant thermal properties within a customizable, open-source framework, but still validation of such model with experimental data is still limited.

In this paper, firstly we briefly describe the mathematical formulation of the Gaussian heat source implementation Section 2 briefly describes the mathematical formulation of the formulation of the Gaussian heat source. Section 3 explains computational setup, mesh setup and material properties. Section 4 presents the simulation results of melt pool dimension and compares them with experimental measurement. Section 5 discusses the implication of the observed agreement and potential future work.

2. Mathematical Model Description

2.1. Energy Equation

LaserbeamFoam application models the energy equation by solving the transient heat equation with a moving Gaussian heat source. The energy equation is as follows:

$$\frac{\partial(\rho\, c_p T)}{\partial t} + \nabla \cdot \left(U \rho\, c_p T\right) - \nabla \cdot (k \nabla T) = q + S_h \qquad (1)$$

where ρ denotes the material density (kg/m^3), and c_p is specific heat capacity at constant pressure ($J/(kg.K)$). T is the local temperature in K. $\mathbf{U}$ is the velocity vector (m/s) of the medium, q is a volumetric heat source term (W/m^3) described

in equation (2) and S_h captures latent-heat release or absorption during phase changes.

2.2. Gaussian Heat Source

The volumetric heat source in this study is described as

$$q = \frac{\Sigma Q}{r^2 \pi \Delta} e^{-\Sigma\left[\left(\frac{x - b_g}{r}\right)^2 + \left(\frac{z - v\,t - l_g}{r}\right)^2\right]} \quad (2)$$

where r denotes the radius of the Gaussian distribution and Q represents the overall beam power. Δ represents the computational cell length scale at which heat is deposited, with 1/Δ being analogous to $|\nabla\alpha|$ in the thin interface constraint. The heat source moves along the positive z-axis (see Figure 2) at a velocity v, initially offset by distances b_g and l_g along the x-axis and z-axis, respectively. Σ is a parameter utilised to portray the beam radius and how concentrated a beam can be, which typically in the range of 1 - 3.

The absorptivity of the heat source depends on the material and is described elsewhere in the literature using Fresnel equations [3]. Figure 1 shows the absorptivity vs the incident angle for SS316L used in this simulation.

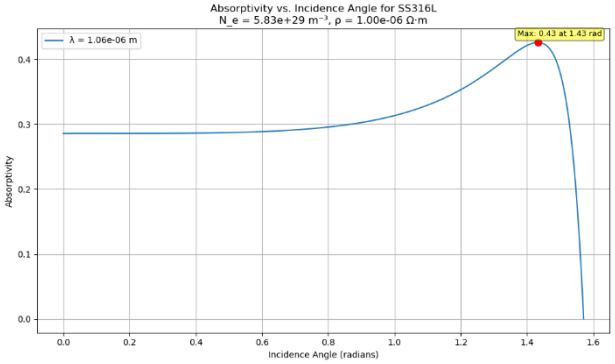

Figure 1. Absorptivity vs the incident angle using Fresnel equations for SS316L stainless steel[3].

2.3. Momentum Equation

The momentum equation that governs the fluid flow in this solver is shown in equation (3)

$$\frac{\partial(\rho\, U)}{\partial t} + \nabla \cdot (\rho\, U \otimes U) = -\nabla P + \nabla \cdot \tau + F_s + F_g + S_m \quad (3)$$

where P is the pressure (Pa), $\boldsymbol{\tau}$ is the viscous stress tensor (Pa), F_s represents surface forces per unit volume (N m⁻³) including recoil forces due to vaporization, $\boldsymbol{F_g}$ describes buoyancy forces and S_m is Carmen-Kozeny sink term to reduce the velocity to zero if it is solid.

2.4. VOF Approach

VOF tracks the metallic phase using volume fraction as an indicator and is described as follow

$$\frac{\partial \alpha}{\partial t} + \nabla \cdot (\alpha \boldsymbol{U}) = 0 \quad (4)$$

where α is the volume indicator of the metallic phase which is between zero and one.

3. Computational Setup

3.1.Geometry And Mesh

A domain size of(600 x 500 x 1000) μm^3 is used for the entire simulation. Out of which stainless-steel substrate is (600 x 350 x 1000) μm^3 ,while the top layer is argon gas. A uniform hexahedral grid mesh of 40 segments across all dimensions is used, which leads to cell size of 15 x 12.5 x 25) μm^3.

3.2.Material Properties

The material properties were setup as per stainless steel 316L and are summarised in Table 1.

Table 1 : Thermo-physical properties of SS316L used in simulation [3,9].

Property	Value
Density (ρ)	7,950 kg/m^3
Thermal Conductivity (κ)	10 $W/m \cdot K$
Heat Capacity (c_p)	500 $J/kg \cdot K$
Solidus (T_s)	1,658 K
Liquidus (T_l)	1,723 K
Latent Heat (L)	2.7×10⁵ J/kg
Volumetric Expansion (β)	5.0×10⁻⁶ K^{-1}

3.3.Process Parameters

In this study, laser heat source parameters were defined to simulate single-track melting of SS316L using LaserbeamFoam. The scanning speed HS_velocity and the laser power HS_Q are similar to those reported experimentally [3] and are summarized in Table 2. A beam radius HS_a of 50 μm was used to match typical spot sizes in literature [10]. Physical constants included a laser wavelength electron number density and electrical resistivity was simulated using the values shown in Figure 1.

Table 2 : Laser properties (power and velocity) used in the simulation to match literature combinations [10]**.**

Case	Q (Power) (W)	Velocity (m/s)
1	260	0.52
2	260	0.87
3	260	1.3
4	260	1.47
5	260	2.2
6	440	1.47
7	620	1.47
8	620	2.07
9	800	2.67

3.4.Solver Settings

The time step was set up to be changing *adjustableRunTime* such that it maintains maximum courant number 0.2 or 0.5 is maintained for stability depending on the cases in Table 2 with the end time to be 2 milliseconds. As for convergence residuals are set at least below 10^{-6} for velocity and below 10^{-9} for the temperature.

4. Simulation Results and Experimental Comparison

4.1.Melt Pool Extraction

Melt pool dimensions were extracted using the temporal statistical data filter with values of epsilon_maximum (maximum value of solid-fluid fraction) higher than 0.5, indicating that full melting has taken place while lower indicating otherwise.

A slice of cross-section of the melt pool is taken at 800 μm from the starting side along the scanning direction, with the width measured perpendicular to scan direction at mid-track; depth measured from surface to maximum penetration. Figure 2 shows a sample cross-section of case 7.

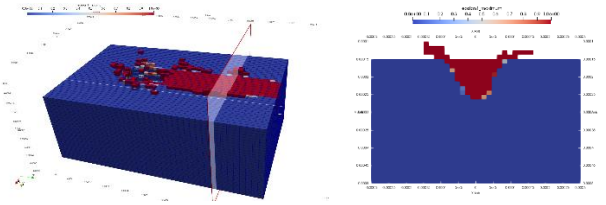

Figure 2. A slice of cross-section of the melt pool slice taken at 800 μm of case 7 of power of 620 W and scanning speed of 1.47 m/s.

4.2.Simulated Results

The simulated results are shown in Table 3 and it shows a decrease of the melt pool depth as the speed increases as in case 1 to 4 ,This behaviour follows the rules of physics: when the scan speed is increases, the amount of time the laser interacts with the material goes is reduced, thus less energy is deposited per unit volume. This means that less material is melting, which makes the melt pools shallower and narrower. This pattern is most clear in the depth of the melt pool, which suggests that depth is more sensitive to changes in energy intake than width in these cases.

Table 3 : Melt pool width and depth for all cases .

Case	Width (μm)	Depth (μm)
1	120	137.5
2	120	87.5
3	120	62.5
4	120	50
5	90	37.5
6	150	87.5
7	150	112.5
8	165	87.5
9	150	75

4.3.Experimental Benchmark

The experimental results are shown in Table 4 indicating both the width and the depth of melt pool on the base plate.

Table 4 : Experimental results reported in [10] **.**

Case	Width (μm)	Depth (μm)
1	114	180
2	125	80
3	85	60
4	94	61
5	83	41
6	98	104
7	130	175
8	125	100
9	160	75

4.4.Comparison of Simulation and Experiment

Table 5 shows a summary of the difference between the experimental and simulated results for the width and depth of the melt pool at different power and scanning speed combinations. The simulated width (120 μm) and depth (137.5 μm) were slightly too high compared to the experimental width (114 μm) and depth (180 μm) at low power (260 W) and low speed (0.52 m/s). The width was off by 5.26% and the depth was off by −23.61%. When the scanning speed goes up (for example, to 2.2 m/s), both the width and depth are too low. The model gets the broad trends correct for higher powers like 440 W and 620 W, but it exhibits larger depth errors, especially at 620 W and 1.47 m/s, where the depth is 35.71%. The closest match is at 800 W and 2.67 m/s, without deviation of the simulated and experimental depths, although the simulation width is slightly lower (the deviation is −6.25%).

Figures 3, 4 and 5 show the simulated and experimental results for three sets of cases: constant power of 260 W at different scan speeds, constant speed of 1.47 m/s at different power levels, and 300 J/m energy density (calculated as power divided by speed). Figure 6 shows a melt pool cross-section from case 1, with the left side showing the simulation and the right side showing the experimental result reported in [10].

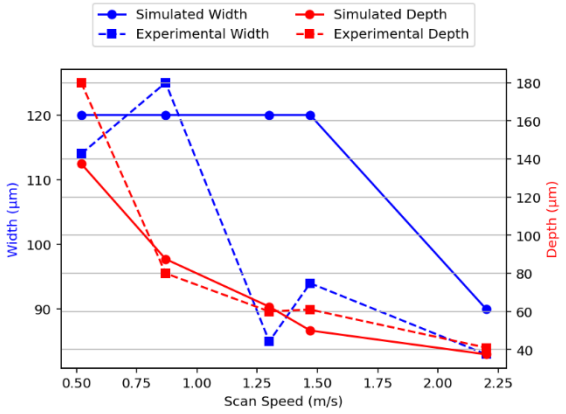

Figure 3. Melt pool dimensions at the power of 260 W and a couples of speeds.

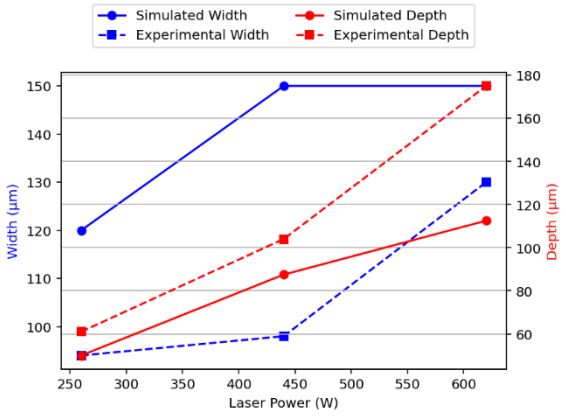

Figure 4. Melt pool dimensions at the scanning speed of 1.47 m/s, and a couple of power sets.

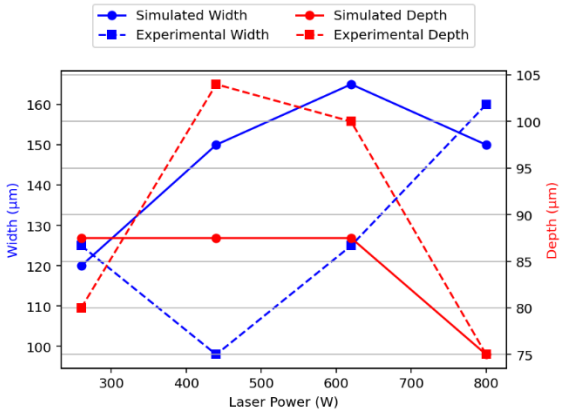

Figure 5. Melt pool dimensions at 300 J/m energy density.

Table 5: Deviation between simulation results in Table 4 and experimental results in Table 3 **.**

Case	Width difference (%)	Depth difference (%)
1	5.26	-23.61
2	-4.00	9.38
3	41.18	4.17
4	27.66	-18.03
5	8.43	-8.54
6	53.06	-15.87
7	15.38	-35.71
8	32.00	-12.50
9	-6.25	0.00

4.5.Computational Cost

The simulated cases were run on razor blade 14 2020 laptop with 8 cores and an AMD Ryzen 9 5900HX processor. The computational time is shown in Table 6 below.

Table 6 **:** Computational time in hours(HH):minutes(MM):seconds(SS) for the cases in Table 2**.**

Case	Simulation time HH:MM:SS
1	02:23:59.48
2	01:46:06.69
3	01:07:20.23
4	01:00:05.05
5	00:53:06.28
6	02:09:05.61
7*	12:59:46.64
8*	04:19:41.86
9	01:29:46.72

*It requires reducing maximum courante number to 0.2 to run the case thus increasing the computational time.

From Table 6 it is observed that significant computational time is required even for the case with a mesh 40^3 size. Reducing the courant number from 0.5 to 0.2 significantly increase computational time as seen in cases 7 and 8 from Table 6.

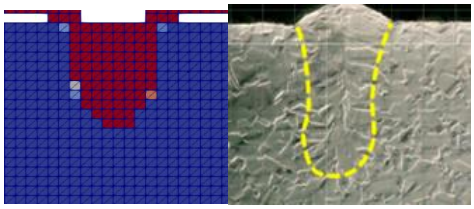

Figure 6. Simulation and experiment [10] comparison of melt-pool cross-section morphology, for laser speed of 0.52 m/s and power of 260 W.

5. Discussion and Outlook

Simulations with LaserbeamFoam showed the similar main patterns as documented in experiments with SS316L single-track melting, where: the width and depth of the melt pool reduced in size as the scan speed increases and the laser power increases. The predicted depth is always within the range of experimental error, but width estimates is slightly overestimated, especially when high energy is applied.

From the examples of 300 J/m energy density vs power in Figure 5, it becomes clear that both width and depth increase with power, but depth is consistently under-predicted in mid-range regimes.

Those inaccuracy may stem from the mesh size so increasing the mesh size might provide different results or our measure error of the melt-pool dimension considering that using temporal data statistics might not capture the proper melt pool morphology as the macro sectional cut of the experimental sample can Moreover, as explained by laserbeamFoam authors, the application over-predict the width due to its simplicity of not accounting for volumetric dilation and vapour plume generation explicitly [3].

Our simulated model accurately shows the qualitative changes in the development of melt pools even with a relatively coarse mesh, such as narrower and shallower pools at higher scanning speeds and larger and deeper pools at higher power. From simulation results, depth predicted comes within a reasonable range of experimental error, although width predictions need to be improved or a better methodology of capturing melt pool should be considered.

As for future works, enabling dynamic absorptivity to vary with temperature and phase changes however those changes come with high computational cost. Another possible improvement is to improve the method of capturing the melt pool morphology in post process.

References

[1] Sampson R, Lancaster R, Sutcliffe M, Carswell D, Hauser C and Barras J 2021. The influence of key process parameters on melt pool geometry in direct energy deposition additive manufacturing systems. *Opt. Laser Technol.* **134** 106609

[2] Wang J, Zhu R, Liu Y and Zhang L 2023. Understanding melt pool characteristics in laser powder bed fusion: An overview of single- and multi-track melt pools for process optimization *Adv. Powder Mater.* **2** 100137

[3] Flint T F, Robson J D, Parivendhan G and Cardiff P 2023 laserbeamFoam: Laser ray-tracing and thermally induced state transition simulation toolkit *SoftwareX* **21** 101299

[4] Flint T F, Robson J D, Esmati P, Grilli N, Parivendhan G and Cardiff P 2024 Version 2.0 — LaserbeamFoam: Laser ray-tracing and thermally induced state transition simulation toolkit *SoftwareX* **25** 101612

[5] King W E, Anderson A T, Ferencz R M, Hodge N E, Kamath C, Khairallah S A and Rubenchik A M 2015 Laser powder bed fusion additive manufacturing of metals; physics, computational, and materials challenges *Appl. Phys. Rev.* **2** 041304

[6] Cao L 2021 Numerical Investigation on Molten Pool Dynamics During Multi-laser Array Powder Bed Fusion Process *Metall. Mater. Trans. A* **52** 211–27

[7] Rai R, Kelly S M, Martukanitz R P and DebRoy T 2008 A Convective Heat-Transfer Model for Partial and Full Penetration Keyhole Mode Laser Welding of a Structural Steel *Metall. Mater. Trans. A* **39** 98–112

[8] Bayat M, Dong W, Thorborg J, To A C and Hattel J H 2021 A review of multi-scale and multi-physics simulations of metal additive manufacturing processes with focus on modeling strategies *Addit. Manuf.* **47** 102278

[9] MatWeb Material Property Data – AISI Type 316L Stainless Steel, annealed and cold drawn bar [Internet]. Available from: https://www.matweb.com/search/datasheet.aspx?matguid=c02b8c0ae42e459a872553e0ebfab648&ckck=1 [Accessed (15 June 2025)].

[10] Zhang Z, Zhang T, Sun C, Karna S and Yuan L 2024 Understanding Melt Pool Behavior of 316L Stainless Steel in Laser Powder Bed Fusion Additive Manufacturing *Micromachines* **15** 170